Check for updates

European Journal of Immunology

Innate Immunity

Basic

Research Article

Innate lymphoid cell characterization in the rat and their correlation to gut commensal microbes

Amanda Sudworth[1], Filip M. Segers[2], Bahtiyar Yilmaz[3], Naomi C. Guslund[4], Andrew J. Macpherson[3], Erik Dissen[5], Shuo-Wang Qiao[4] and Marit Inngjerdingen[1,2]

[1] Department of Pharmacology, Institute of Clinical Medicine, University of Oslo, Oslo, Norway
[2] Department of Pharmacology, Oslo University Hospital, Oslo, Norway
[3] Department of Visceral Surgery and Medicine, Inselspital, Bern University Hospital, Bern, Bern, Switzerland
[4] Department of Immunology, Institute of Clinical Medicine, University of Oslo, Oslo, Norway
[5] Department of Molecular Medicine, Institute of Basic Medical Sciences, University of Oslo, Oslo, Norway

Innate lymphoid cells (ILCs) are important for tissue immune homeostasis, and are thoroughly characterized in mice and humans. Here, we have performed in-depth characterization of rat ILCs. Rat ILCs were identified based on differential expression of transcription factors and lack of lineage markers. ILC3s represented the major ILC population of the small intestine, while ILC2s were infrequent but most prominent in liver and adipose tissue. Two major subsets of group 1 ILCs were defined. Lineage$^-$T-bet$^+$Eomes$^+$ cells were identified as conventional NK cells, while lineage$^-$T-bet$^+$Eomes$^-$ cells were identified as the probable rat counterpart of ILC1s based on their selective expression of the ILC marker CD200R. Rat ILC1s were particularly abundant in liver and intestinal tissues, and were functionally similar to NK cells. Single-cell transcriptomics of spleen and liver cells confirmed the main division of NK cells and ILC1-like cells, and demonstrated Granzyme A as an additional ILC1 marker. We further report differential distributions of NK cells and ILCs along the small and large intestines, and the association of certain bacterial taxa to frequencies of ILCs. In conclusion, we provide a framework for future studies of ILCs in diverse rat experimental models, and novel data on the potential interplay between commensals and intestinal ILCs.

Keywords: NK cells · ILC · microbiome · rat

Additional supporting information may be found online in the Supporting Information section at the end of the article.

Introduction

Innate lymphoid cells (ILCs) provide host defense against infection and contribute to tissue homeostasis and repair. They mediate most of their effector functions through regulatory cytokines. ILCs are generally divided into four groups—conventional NK cells, ILC1s, ILC2s, and ILC3s [1]. ILCs are particularly numerous under mucosal epithelia and in nonlymphoid tissues such as the liver, lung, skin, and uterus [2]. While NK cells can circulate between tissues, ILC1s, ILC2s, and ILC3s are predominantly tissue resident under normal physiological conditions [3].

Correspondence: Dr. Marit Inngjerdingen
e-mail: mariti@medisin.uio.no

© 2022 Wiley-VCH GmbH

This is an open access article under the terms of the Creative Commons Attribution-NonCommercial License, which permits use, distribution and reproduction in any medium, provided the original work is properly cited and is not used for commercial purposes.

source: https://doi.org/10.48350/176897 | downloaded: 13.1.2023

15214141, 2022, 5, Downloaded from https://onlinelibrary.wiley.com/doi/10.1002/eji.202149639 by Universitat Bern, Wiley Online Library on [05/01/2023]. See the Terms and Conditions (https://onlinelibrary.wiley.com/terms-and-conditions) on Wiley Online Library for rules of use; OA articles are governed by the applicable Creative Commons License

ILC groups are defined by the absence of lineage markers for other immune cells, and expression of defining membrane markers and transcription factors. NK cells and ILC1s both produce IFN-γ in response to cytokines. NK cells possess lytic function, as ILC1 subsets does that express low levels of CD127 and high levels of granzymes [4–6]. ILC1s have a phenotype closely resembling NK cells. Both cell types express the transcription factor T-bet, but only NK cells express the transcription factor Eomes [7]. In mice, both ILC1s and NK cells express NKp46 and NKR-P1C (NK1.1, only expressed in C57/Bl6 and Bl/10). The similarities between ILC1s and circulating versus tissue-resident NK cells complicate clear assignments to either cell type [7, 8]. Further complicating the issue, NK cells coexist in distinct developmental stages [9]. Both ILC1s and tissue-resident NK cells express markers associated with tissue residency such as CD49a, CD103, and CXCR6 [10]. While ILC2s and ILC3s express the IL-7 receptor alpha (IL-7Rα; CD127), it is expressed by ILC1s in a tissue-dependent manner. CD127 is absent from mouse NK cells but expressed by human CD56^{bright} NK cells [11].

ILC2s are defined by high expression levels of the transcription factor GATA-3. They primarily produce the Th2-cytokines IL-4, IL-5, and IL-13 in response to IL-25, IL-33, and/or thymic stromal lymphopoietin, and thereby contribute to type 2 immune responses [1]. ILC2s express the IL-33 receptor, ST2, and the prostaglandin D2 receptor 2 (the latter only expressed by human ILC2s) [12]. ILC2s are found in skin of both humans and mice, and in lower numbers in blood and intestines. While ILC2s are a dominant ILC population in mouse lungs, they are only marginally detected in human lungs [13, 14].

ILC3s are heterogeneous and can be subdivided into CCR6$^+$ lymphoid tissue-inducer cells, natural cytotoxicity receptor (NCR)$^+$ cells, as well as "ex-ILC3s" that have shifted toward an ILC1 phenotype. ILC3s are characterized by their expression of the transcription factor RORγt and the aryl hydrocarbon receptor. ILC3s produce IL-17 and/or IL-22 in response to cytokines like IL-1β and IL-23. ILC3s are the dominant ILC population within the intraepithelial compartment and the lamina propria (LP) of the small intestine in both humans and mice. Here, they are functionally dependent on commensal microbes [15, 16], but also able to regulate microbial homeostasis via production of IL-22 [17, 18].

We have previously thoroughly characterized rat NK cells and NK cell subsets [19–22], but ILCs, and in particular ILC1s, have not been systematically characterized so far in the rat. Rat NK cells are defined as NKp46$^+$ [23] or CD3$^-$NKR-P1A$^+$, where rat NKR-P1A is a functional homologue to mouse NKR-P1C. Considering renewed interest in rat as an immunological research animal model, we set out to define and characterize rat innate lymphocyte populations. We combined phenotypic flow cytometry analyses, single- cell transcriptomics, and functional assays to distinguish and characterize innate lymphocytes in the rat.

Results

Rat ILC1s, ILC2s, and ILC3s are defined by transcription factors and function

To identify rat ILCs, we followed a strategy based on lack of lineage markers (Lin$^-$ cells; excluding T cells [CD3$^+$], B cells [Ig kappa chain$^+$], and monocytes, macrophages, granulocytes, DCs [all positive for SIRP-α in rats]), and differential expression of CD127 and transcription factors Eomes, T-bet, GATA-3, or RORγt. In spleen, Lin$^-$CD127$^+$ cells contain subsets with high or dim CD127 expression levels (also observed in blood but not in other tissues [data not shown]) (Fig. 1A). From within the CD127^{high} gate, we identified putative ILC2s and ILC3s as GATA-3^{high} or RORγt$^+$ cells, while ILC1s were identified as T-bet$^+$Eomes$^-$ (Fig. 1A). Within Lin$^-$CD127^{dim} spleen cells, were found predominantly NK cells (T-bet$^+$Eomes$^+$) and minor frequencies of ILC1s (T-bet$^+$Eomes$^-$) and ILC3s. Finally, NK cells (T-bet$^+$Eomes$^+$) were identified within the Lin$^-$CD127$^-$ gate, along with T-bet$^+$Eomes$^-$ cells (Fig. 1A). We confirmed mRNA transcripts for IL-5 or IL-22 within liver Lin$^-$CD127$^+$GATA-3^{high} cells or spleen Lin$^-$CD127$^+$RORγt$^+$ cells, respectively, upon PMA/ionomycin stimulation. (Fig. 1B and D). Further, we show that Lin$^-$CD127$^-$T-bet$^+$Eomes$^-$ spleen cells produced IFN-γ and degranulated in response to tumor targets at comparable levels to spleen NK cells (Fig. 1C and E).

Rat NK cells are traditionally defined as NKR-P1A$^+$CD3$^-$ cells. However, around 15% of spleen Lin$^-$NKR-P1A$^+$ cells lacked Eomes (Fig. 1F), suggesting that ILCs also fall into this gate. Moreover, we previously described an NK cell subset expressing high levels of the inhibitory receptor NKR-P1B that was distinct from conventional NK cells [21]. We show here that NKR-P1B^{bright} cells are mainly Eomes negative (Fig. 1G), suggesting they may be ILC1s.

Rat ILCs share a core signature independent of their tissue localization

We next tested the tissue distribution and phenotypes of the identified rat ILC populations by flow cytometry. Lin$^-$T-bet$^+$Eomes$^+$ NK cells were found in expected tissues as previously reported for CD3$^-$NKR-P1A$^+$ NK cells (Fig. 2A). Lin$^-$T-bet$^+$Eomes$^-$ were found in most tissues tested, and in very high frequencies in the liver (Fig. 2B). CD127$^+$ ILC1s were barely detected in any tissue (Supporting information Fig. S1A). ILC2s were mainly located in liver, adipose tissue, small intestines, and lung (Fig. 2C), while ILC3s were most abundant within the small intestinal LP, lungs, and skin (Fig. 2D). Our data on intestinal ILC3s align with studies in mice and humans, but contrast with a previous study in rat where ILC2s were identified as the most abundant intestinal ILC [24]. We additionally profiled Sprague–Dawley (SPD) and Wistar Kyoto (WKY) rats, and found that ILC3s were the dominant intestinal ILCs in these strains (Supporting information Fig. S1B and C).

© 2022 Wiley-VCH GmbH

15214141, 2022, 5, Downloaded from https://onlinelibrary.wiley.com/doi/10.1002/eji.202149639 by Universitat Bern, Wiley Online Library on [05/01/2023]. See the Terms and Conditions (https://onlinelibrary.wiley.com/terms-and-conditions) on Wiley Online Library for rules of use; OA articles are governed by the applicable Creative Commons License

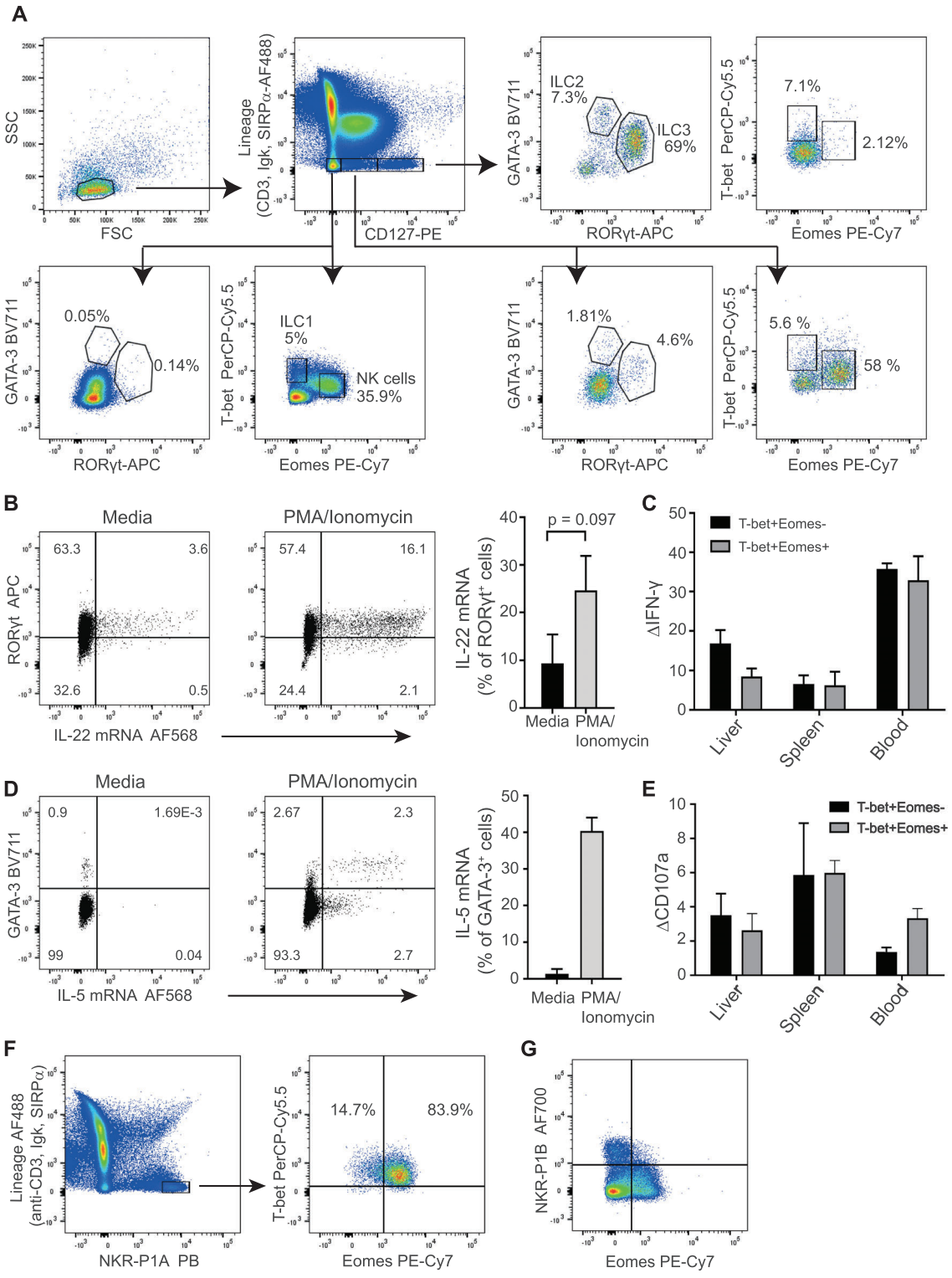

Figure 1. Definition of rat ILCs. (A) Gating strategy for definition of rat ILCs in spleen. IL-22 mRNA production by Lin$^-$CD127$^+$Rorγt$^+$ ILC3s from small intestinal LP (B) or IL-5 mRNA production by Lin$^-$CD127$^+$GATA-3^{high} ILC2s from liver (D) assessed by PrimeFlow in mononuclear cells from the lamina propria of small intestine with/without PMA and ionomycin stimulation for 4 h. Representative of three independent experiments. Percentage of IFN-γ in response to PMA/ionomycin (C) or degranulation in response to YAC-1 tumor targets (E) in Lin-T-bet$^+$Eomes$^+$ NK cells (grey bars) or Lin-T-bet$^+$Eomes$^-$CD127$^{+/-}$ cells (black bars) in liver, spleen, or blood. Data represent the mean of three independent experiments ± SD. Degranulation is represented as ΔCD107a; the difference between CD107a expression measured against targets versus no targets. (F) Expression of transcription factors Eomes, T-bet, Rorγt, and Gata-3 within Lin$^-$NKR-P1A$^+$CD3$^-$ NK cells in spleen, demonstrating that a fraction of these lack Eomes. (G) Lin$^-$CD127$^{+/-}$NKR-P1B^{bright} cells in blood express low levels of Eomes.

© 2022 Wiley-VCH GmbH

15214141, 2022, 5, Downloaded from https://onlinelibrary.wiley.com/doi/10.1002/eji.202149639 by Universitat Bern, Wiley Online Library on [05/01/2023]. See the Terms and Conditions (https://onlinelibrary.wiley.com/terms-and-conditions) on Wiley Online Library for rules of use; OA articles are governed by the applicable Creative Commons License

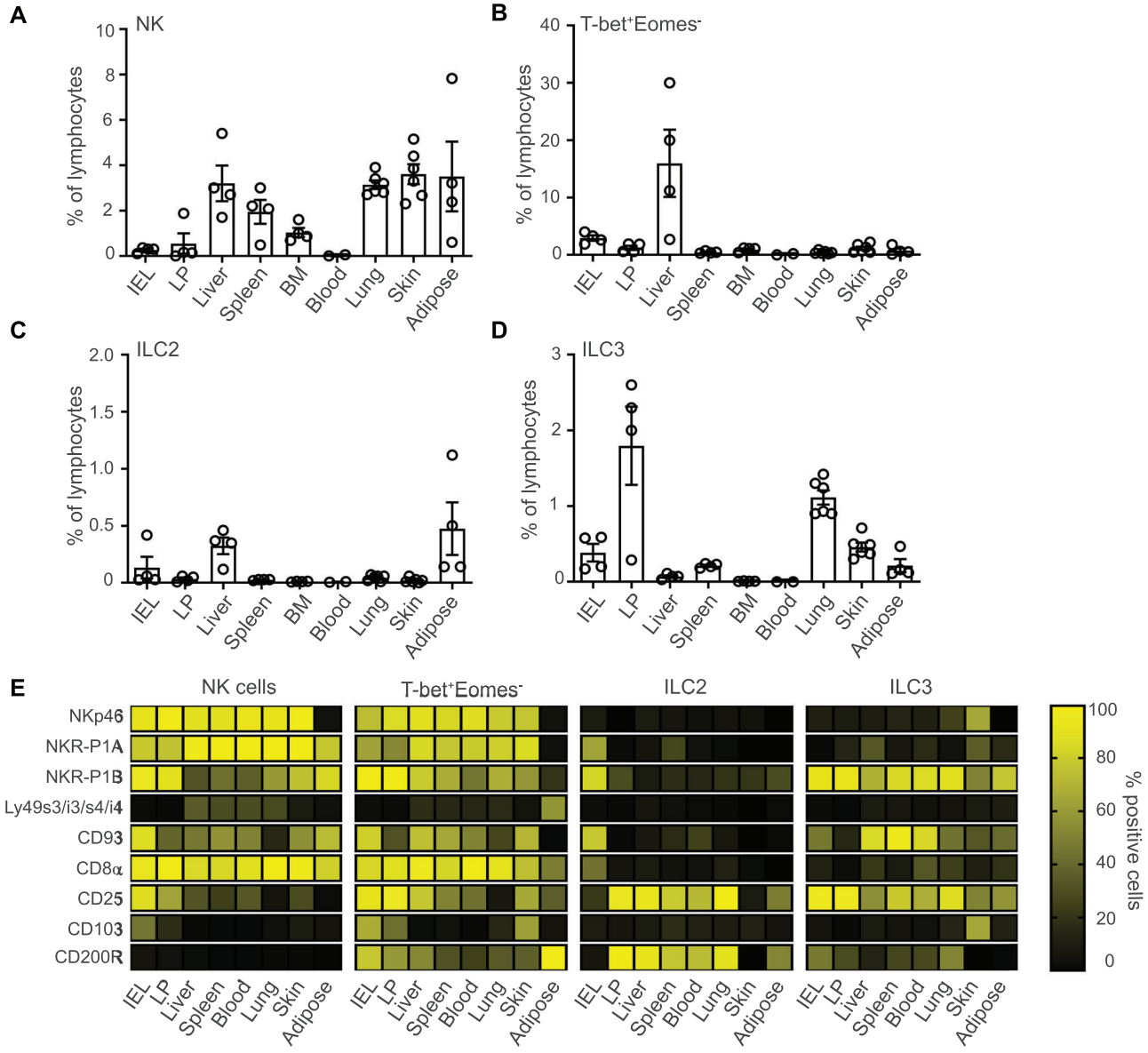

Figure 2. Tissue distribution and phenotypic profile of rat ILCs. Frequencies of Lin-T$^-$bet$^+$Eomes$^+$ NK cells (A), Lin-T-bet$^+$Eomes$^-$CD127$^{+/-}$ ILC1s (B), Lin$^-$CD127$^+$GATA-3^{high} ILC2s (C), Lin$^-$CD127$^+$Rorγt$^+$ ILC3s (D) in indicated tissues presented as percentage of lymphocytes. Data are presented as the mean of three to five independent experiments per tissue ± SD. (E) Heatmap showing percentage of cells expressing indicated markers within Lin$^-$T$^-$bet$^+$Eomes$^+$ NK cells, Lin$^-$T-bet$^+$Eomes$^-$CD127$^{+/-}$ cells, Lin$^-$CD127$^+$GATA-3^{high} ILC2s, and Lin$^-$CD127$^+$Rorγt$^+$ ILC3s. The data are presented as the mean of three to five independent experiments.

The phenotypic profiles of ILCs across tissues were next compared by flow cytometry. ILC2s expressed typical NK cell receptors at low frequencies, but distinctly expressed CD25 and CD200R in most tissues (Fig. 2E and Supporting information Fig. S2A-C). ILC3s generally expressed low amounts of activating receptors, NKp46 and NKR-P1A, but strongly expressed the inhibitory receptor NKR-P1B and the C-type lectin receptor CD93. Similarly to ILC2s, ILC3s expressed both CD25 and CD200R. The phenotype of Lin$^-$T-bet$^+$Eomes$^-$ cells largely mirrored NK cells, except stronger expression of CD25 and NKR-P1B, and exclusive expression of CD200R. The markers, CD49a and CD49b, distinguish between NK cells and ILC1s/tissue-resident NK cells in the mouse, but were heterogeneously expressed by both subsets in rats (Supporting information Fig. S2D).

Single-cell RNA sequencing reveals subsets of group 1 ILCs

To further differentiate between NK cells and putative ILC1s, scRNA-Seq was undertaken in liver and spleen mononuclear cells enriched for innate lymphocytes. Unfortunately, transcription fac-

© 2022 Wiley-VCH GmbH

15214141, 2022, 5, Downloaded from https://onlinelibrary.wiley.com/doi/10.1002/eji.202149639 by Universitat Bern, Wiley Online Library on [05/01/2023]. See the Terms and Conditions (https://onlinelibrary.wiley.com/terms-and-conditions) on Wiley Online Library for rules of use; OA articles are governed by the applicable Creative Commons License

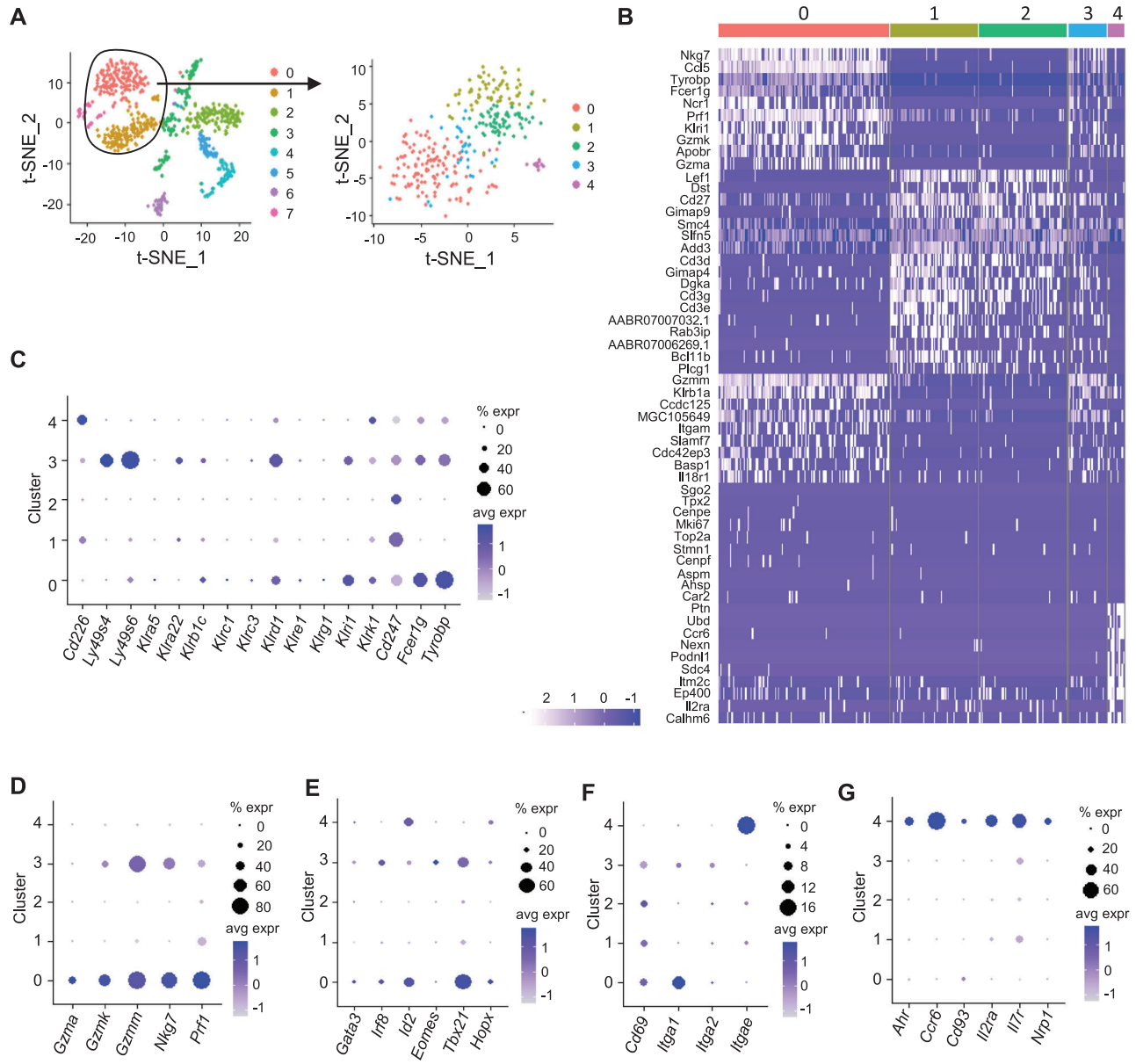

Figure 3. NK cells, ILC1s, and ILC3s defined in spleen by single-cell transcriptomics. (A) *t*-SNE plot of 689 spleen cells enriched for innate lymphocytes, showing subsetting and reclustering of lymphocytes leading to identification of five clusters. (B) Heatmap of the top 10 differentially expressed genes in each cluster. (C-G) Dot plots showing detection rate and average gene expression of indicated genes within the defined clusters.

tors *Eomes*, *Gata3*, and *Rorc* were poorly expressed in the dataset, precluding their use to define ILC subsets. Innate lymphcoytes were, therefore, identified based on expression of *Klrb1a* (NKR-P1A) and/or *Ncr1* (NKp46), and exclusion of other lineage markers (Supporting information Fig. S3A and B). Five subclusters were identified in spleen (Fig. 3A and B). Clusters 0 and 3 were identified as putative NK cells/ILC1s. Cluster 0 expressed more transcripts for *Tbx21*, adapters for activating receptors (*Tyrobp* and *Fcer1g*), and cytotoxic granule components (*Gzma, Gzmk, Nkg7*, and *Prf1*) (Fig. 3C-F). We conclude that cluster 0 likely represented conventional NK cells, and that cluster 3 may represent ILC1s. Finally, cluster 4 was enriched for transcripts associated to ILC3s (Fig. 3G).

Three clusters of innate lymphocytes were identified in liver (Fig. 4A and B). In contrast to spleen, these clusters had more distinct profiles. Cluster 0 contained low levels of NK-cell receptor transcripts and cytolytic molecules, but was enriched for *GzmA, Itga1*, *Cd93*, *Il2ra*, and *Il18r1* (Fig. 4C-I). This profile is reminiscent of mouse liver ILC1s, and could represent the large population of CD127$^-$ ILC1s that we detect by flow cytometry. Clusters 1 and 2 showed differential expression of NK cell receptor transcripts and cytolytic molecules, with particularly *Klrg1* enriched

© 2022 Wiley-VCH GmbH

15214141, 2022, 5, Downloaded from https://onlinelibrary.wiley.com/doi/10.1002/eji.202149639 by Universitat Bern, Wiley Online Library on [05/01/2023]. See the Terms and Conditions (https://onlinelibrary.wiley.com/terms-and-conditions) on Wiley Online Library for rules of use; OA articles are governed by the applicable Creative Commons License

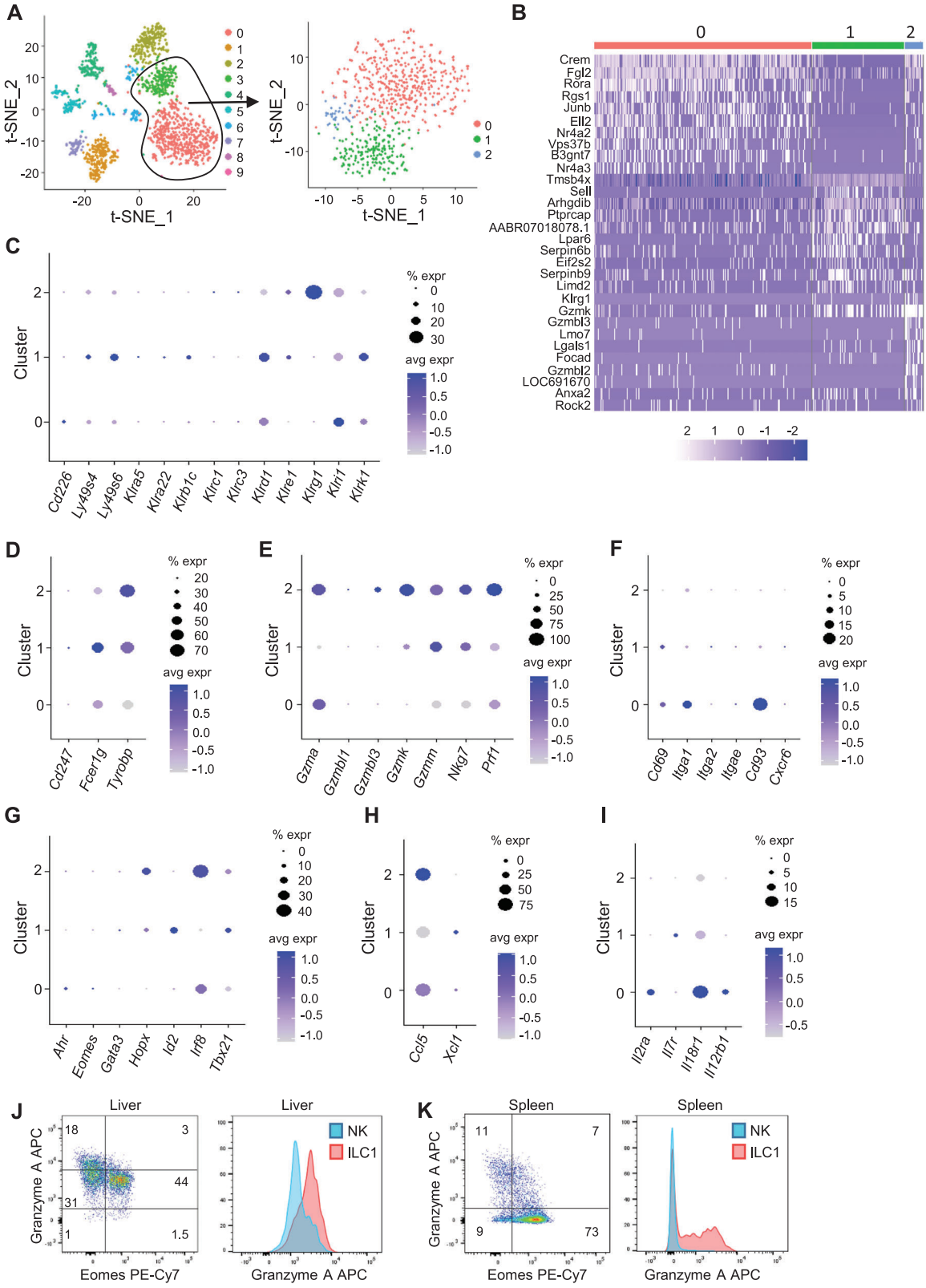

Figure 4. Three group 1 ILC populations in liver defined by single-cell transcriptomics. (A) *t*-SNE plot of 1577 liver cells enriched for innate lymphocytes, showing subsetting and reclustering of lymphocytes leading to identification of three clusters. (B) Heatmap of the top 10 differentially expressed genes in each cluster. (C-I) Dot plots showing detection rate and average gene expression of indicated genes within the three clusters. (J-K) Granzyme A expression within Lin$^-$T-bet$^+$Eomes$^-$CD127$^{+/-}$ cells (red) or Lin$^-$T$^-$bet$^+$Eomes$^+$ NK cells (blue) determined via flow cytometry of liver (J) or spleen (K) cells. Representative of three experiments.

© 2022 Wiley-VCH GmbH

15214141, 2022, 5, Downloaded from https://onlinelibrary.wiley.com/doi/10.1002/eji.202149639 by Universitat Bern, Wiley Online Library on [05/01/2023]. See the Terms and Conditions (https://onlinelibrary.wiley.com/terms-and-conditions) on Wiley Online Library for rules of use; OA articles are governed by the applicable Creative Commons License

1521414, 2022, 5, Downloaded from https://onlinelibrary.wiley.com/doi/10.1002/eji.202149639 by Universitat Bern, Wiley Online Library on [05/01/2023]. See the Terms and Conditions (https://onlinelibrary.wiley.com/terms-and-conditions) on Wiley Online Library for rules of use; OA articles are governed by the applicable Creative Commons License

in cluster 2. These two clusters, thus, likely represent different NK cell subsets. ILC2s or ILC3s were not identified in this dataset. *GzmA* stood out as a marker to distinguish NK cells from ILC1s in liver and spleen, and we confirmed by flow cytometry, this distinction by demonstrating high Granzyme A levels in liver and spleen ILC1s compared to NK cells (Fig. 4J and K).

Biogeography of ILCs and their association to microbiota in the intestinal compartment

During the initial characterization of ILCs, we observed relatively high heterogeneity in frequencies of ILCs from small intestine compared to other tissues. We therefore compared ILC frequencies along the intestinal tract with matched analysis of the commensal microbiota. The analysis was based on six male PVG littermate rats, and an additional three age-matched female PVG.7B littermates. NK cells were more frequent in LP than within the intraepithelial lymphocytes (IEL), increasing in frequencies toward the colon (Fig. 5A). Lin$^-$T-bet$^+$Eomes$^-$ cells were more abundant than NK cells, and with no segmental dominance. ILC3s showed a clear trajectory of high frequency in the jejunum that declined sharply toward the colon. No apparent segregation of rats from the different cages was observed with respect to NK cells, ILC3s, or Lin$^-$T-bet$^+$Eomes$^-$ cells. Like NK cells, ILC2s showed preferential localization to the LP, but an almost complete lack of ILC2s was observed among the PVG.7B rats. We have observed this lack of ILC2s as a cage-specific factor, irrespective of strain, sex, or age, and suspect that this effect is shaped by the microbiome. In support, we observed differences in abundance of a number of bacterial species between the PVG and PVG.7B rats in cecum and ileum (colon was omitted from this analysis due to lack of fecal contents in one PVG.7B rats) (Supporting information Fig. S4). Interindividual differences in abundance of certain bacterial strains and of bacterial richness were apparent (Fig. 5B and C). Alpha diversity analysis with Shannon and Simpson indices showed a higher bacterial richness in the cecum and colon. Beta diversity analysis show that the samples cluster mainly by either small or large intestine (Fig. 5D). For colon and cecum, we observe a tendency that rats housed in the same cage cluster, together indicating cage effects on the abundance of a number of bacterial species. This segregation was strongest for the three female rats, compared to the six littermate males.

We found little correlation between bacterial diversity with frequencies of ILCs in any segment of the gut, with exception of ILC2s among ileal IEL and NK cells among jejunal IEL (Fig. 5E). However, we found associations between certain taxa and ILC frequencies in the cecum and colon. In particular, the Coriobacteriales and the Bacteriodales family (*Prevotellaceae* and *Prevotella*) were positively correlated to Lin$^-$T-bet$^+$Eomes$^-$ cells, ILC2, and ILC3 in cecum (Fig. 5F), while in colon ILC2s correlated to Coriobacteriaceae and ILC3s to Lachnospiraceae (Fig. 5G). IEL colonic NK cells were significantly correlated to *Clostridia* and *Proteobacteria* species (unclassified taxa) (Fig. 5F), and to *Parabacteroides* and an unclassified taxa of *Peptococcaceae* in cecum (Fig. 5H).

Discussion

We provide here an in-depth analysis of rat ILCs. Our study shows that while rat ILC2s and ILC3s are readily identified across different tissues, the definition of rat ILC1s is less straightforward. We clearly observed two main populations of group 1 ILCs by flow cytometry that were either Lin$^-$T-bet$^+$Eomes$^-$ or Lin$^-$T-bet$^+$Eomes$^+$. Eomes is a marker for NK cells, and we could readily verify that the Lin$^-$T-bet$^+$Eomes$^+$ cells represent conventional rat NK cells. We found very little expression of CD127 by Lin$^-$T-bet$^+$Eomes$^-$ cells. Although CD127 is a defining marker for mouse ILC1s, CD127 can be variably expressed by ILC1s in certain tissues [7], and it is not a reliable marker for human ILC1s [25, 26]. We found Lin$^-$T-bet$^+$Eomes$^-$ in most tissues tested, and most prominently in the liver. In humans and mice, the liver harbors tissue-resident NK cells that are distinguishable from circulating NK cells as being Eomes$^{lo/-}$ and positive for markers for tissue residency [27, 28]. Certainly, the ability of rat liver Lin$^-$T-bet$^+$Eomes$^-$ to degranulate in response to tumor targets could argue that the cells represent tissue-resident NK cells, as ILC1s are thought to possess little cytolytic activity. Of note, the minor fraction of CD127$^+$ cells among the Lin$^-$T-bet$^+$Eomes$^-$ cells showed lack of degranulation against tumor targets (data not shown), indicating the existence of a minor noncytolytic ILC1 subset.

Further, we found by flow cytometry that CD200R was selectively expressed by Lin$^-$T-bet$^+$Eomes$^-$CD127$^{+/-}$ cells but not by Lin$^-$T-bet$^+$Eomes$^+$ cells. CD200R was previously shown to selectively mark ILCs but not conventional NK cells in the mouse [29]. Additionally, we found through our scSeq data, a skewed expression of Granzyme A within putative ILC1s, which was also confirmed by flow cytometry. This is nicely in line with a recent study demonstrating high Granzyme A expression by liver ILC1s in the mouse [4], although mouse NK cells express more Granzyme A than rat NK cells. We thus propose to define conventional rat NK cells as Lin$^-$T-bet$^+$Eomes$^+$CD200R$^-$GranzymeA$^{-/low}$ and rat ILC1s as Lin$^-$T-bet$^+$Eomes$^-$CD127$^{+/-}$CD200R$^+$GranzymeA^{high}. The ontogenic relationship between NK cells and ILC1s is unclear, but it has been proposed that ILC1s stem from a separate precursor than NK cells downstream of the common lymphoid progenitor [1, 30]. With currently available tools in the rat, we are unable to address the ancestral relationship between rat ILC1s and NK cells.

The putative inhibitory receptor NKR-P1A (CD161) is a marker for ILCs in humans alongside CD127. A functional homologue of human NKR-P1A is not defined in rodents, but the inhibitory receptor NKR-P1B represents the dominant inhibitory NKR-P1 receptor in the rat [19, 31]. We previously showed that NKR-P1B is expressed by almost all NKR-P1A$^+$CD3$^-$ lymphocytes among intestinal IEL, and highly expressed by a cytolytic subset of NKR-P1A$^+$CD3$^-$ cells in blood, liver, and lungs [21]. We previously thought that these cells represented a subset of conventional NK cells, but showing here their lack of Eomes, we redefine them as ILC1s. Further, we show by flow cytometry that NKR-P1B is also highly expressed by rat ILC3s, and at lower frequencies in ILC2s. This is akin to a study in mice, showing a high frequency of NKR-P1B on mouse intestinal NK cells/ILC1s and ILC3, but low expres-

© 2022 Wiley-VCH GmbH

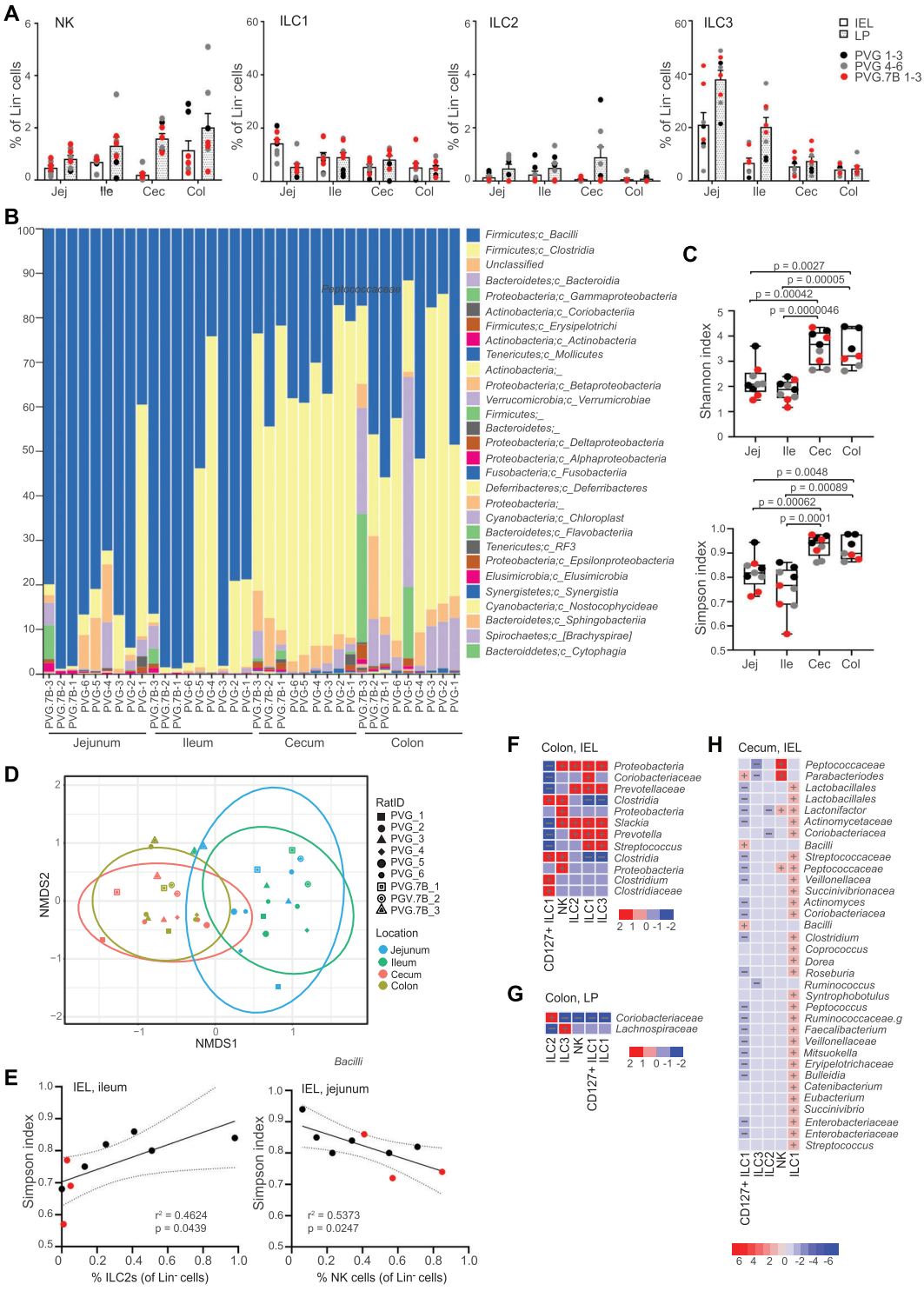

Figure 5. Correlation ILC frequencies with intestinal microbiota. (A) Percentage of Lin⁻T⁻bet⁺Eomes⁺ NK cells, Lin⁻T-bet⁺Eomes⁻CD127$^{+/-}$ cells, Lin⁻CD127⁺GATA-3^{high} ILC2s, Lin⁻CD127⁺Rorγt⁺ ILC3s within IELs (white bars) or LP (dotted bars) in indicated gut segments. PVG rats (n = 6) are color-coded black and grey (two cages), PVG.7B rats (n = 3) are color-coded red. (B) Relative abundance of genera identified in jejunum, ileum, cecum, and colon, based on taxonomic assignment of 16S rDNA sequences. (C) Alpha diversity measured by Shannon and Simpson indices in different gut segments. PVG rats (n = 6) are color-coded black and grey (two cages), PVG.7B rats (n = 3) are color-coded red. (D) Beta diversity analysis of the nine individual rats across jejunum, ileum, cecum, and colon. (E) Scatterplots of bacterial diversity with ILC2 (left panel) or NK cell (right panel) frequencies in the indicated gut segment. (F-H) Heatmaps showing association between bacterial species and ILC frequencies among IEL in colon (F), in colon LP (G), and among IEL in cecum (H) and p value < 0.05 and adj-p value < 0.3. *, indicates unclassified taxa. Color code on heatmaps shows the effect size calculated by using MaAsLin2. Positive values are positively associated with increasing relative abundance of bacteria and negative values negatively associated with reducing relative abundance of bacteria.

© 2022 Wiley-VCH GmbH

15214141, 2022, 5, Downloaded from https://onlinelibrary.wiley.com/doi/10.1002/eji.202149639 by Universität Bern, Wiley Online Library on [05/01/2023]. See the Terms and Conditions (https://onlinelibrary.wiley.com/terms-and-conditions) on Wiley Online Library for rules of use; OA articles are governed by the applicable Creative Commons License

15214141, 2022, 5, Downloaded from https://onlinelibrary.wiley.com/doi/10.1002/eji.202149639 by Universitat Bern, Wiley Online Library on [05/01/2023]. See the Terms and Conditions (https://onlinelibrary.wiley.com/terms-and-conditions) on Wiley Online Library for rules of use; OA articles are governed by the applicable Creative Commons License

sion of ILC2s [32]. Unfortunately, NKR-P1B was not identified in our single-cell RNA dataset as gene annotations were based on the available BN genome, which contains another allelic variant of NKR-P1B than the PVG strain. The functional significance of NKR-P1B by ILCs is currently unknown.

Lung tissues in the rat were mainly populated by NK cells, ILC1s, and ILC3s, which is similar to humans [33], while mouse lungs are predominantly populated by ILC2s [34]. The small intestine was dominated by ILC3s, which is in line with studies in mice and humans [35, 36]. ILC2s were present at very low frequencies or even undetectable in the intestines as in humans [36]. In contrast, a previous study investigating ILCs in SPD, BN, and LEW rats reported that ILC2s, and not ILC3s, dominate intestinal tissue [24]. Our own analysis of SPD rats shows a dominance of ILC3s in the intestine as observed for the PVG rats. The PVG and SPD rats used in our study were obtained from two different animal facilities, we thus, find it unlikely that our results are skewed by the microbiome. We cannot exclude, however, that differences in microbiota in the animal facilities may explain the contradictory results.

ILCs, and in particular ILC3s, are thought to be important for regulating intestinal immune homeostasis by interplaying with commensal microbes [37]. We found relatively large variations in frequencies of ILC1s and ILC2s compared to ILC3s in the different gut segments. This could potentially reflect that ILC1s and ILC2s could be more sensitive to fluctuations in the composition of the commensal microbiome than ILC3s. The microbiota certainly influences the frequencies of immune cells in the intestines, and *Clostridia* are shown to induce Tregs [38], while segmented filamentous bacteria induce Th17 cells [39]. There are only a few studies that link particular bacterial strains with ILCs. ILC2s numbers in the stomach was shown to be directly correlated to the S24-7 taxa of Bacteroidetes [40]. Germ-free mice contain larger proportions of ILC2s than colonized mice [41], indicating a negative influence of the commensal microbiota, perhaps explaining the normally low frequencies of ILC2s in the gut. Interestingly, we observed opposing associations of ILC2s and ILC3s with Lachnospiraceae of the *Clostridia* order. These produce short-chain fatty acids that may act on Ahr. Ahr was recently shown to negatively regulate ILC2s, while promoting ILC3s [42]. We found positive correlations between ILC1, ILC2, and ILC3 with the *Prevotella* genus. Similarly, human intestinal $NKp44^{+}CD56^{-}$ ILCs were found to correlate to the *Prevotellaceae* family in a group of HIV-1 infected individuals [43]. NK cells were positively correlated to *Proteobacteria* and *Clostridia* variants in the colon. How these bacterial strains may affect NK cells is not known, but interestingly, recombinase A peptide sequence from *Proteobacteria* has been shown to be recognized by the NK cell receptor KIR2DS4 via HLA-C in humans [44], but whether a similar system operates in the rat is uncertain.

In conclusion, we have identified ILC1s, ILC2s, and ILC3s in the rats. NK cells and ILC1s share many phenotypical and functional attributes, but form distinct populations in all tissues tested, and can be distinguished based on Eomes, CD200R, and Granzyme A expression. We further find correlations of NK cell and ILC frequencies with certain bacterial strains in cecum and colon that warrant further studies.

Materials and methods

Rats

Male or female rats aged 8 to 20 weeks of the inbred strains PVG, PVG.7B, SPD, or WKY were used. The PVG.7B congenic strain carries the CD45 allele RT7.2 on the PVG (RT7.1) genetic background, and were used interchangeably with PVG rats. The PVG, PVG.7B, and WKY rats have been maintained at the Department of Comparative Medicine, Institute of Basic Medical Sciences, University of Oslo, for more than 30 generations. SPD rats have been bred at the Department of Comparative Medicine, Oslo University Hospital. PVG/PVG.7B were used throughout unless otherwise specified. Feeding, monitoring, handling, and sacrifice of animals were done in compliance with regulations set by the Ministry of Agriculture of Norway and "The European Convention for the Protection of Vertebrate Animals used for Experimental and other Scientific Purposes." The laboratory animal facilities are subject to a routine health-monitoring program and tested for infectious organisms according to a modification of Federation of European Laboratory Animal Science Associations recommendations. Rats were sacrificed by controlled asphyxiation with CO_2.

Tissue homogenization and isolation of mononuclear cells

Mononuclear cells were prepared from blood via density gradient separation on Lymphoprep (Axis-Shield, Norway), and from spleen and lungs by crushing through a 70-μm cell strainer followed by density-gradient separation on Lymphoprep. IEL were isolated from the small intestine as previously described [45, 46], followed by isolation of LP lymphocytes by rinsing intestinal pieces in ice-cold PBS, and incubation in cRPMI with 1.6 mg/mL type IV collagenase (Worthington Biochemical Corporation) for 30 min at 37°C, filtering, and Lymphoprep separation. Skin lymphocytes were isolated as previously described [47]. Liver cells were separated by crushing through 70 μm filters, Lymphoprep separation, and removal of macrophages by 1 h incubation in cell culture flasks at 37°C. Visceral adipose tissue was incubated in cRPMI with 1.6 mg/mL type IV collagenase for 30 min at 37°C, filtered, and washed in PBS with 2% FBS.

Antibodies and flow cytometry

Flow cytometry experiments were executed according to guidelines [48]. Antibodies and conjugates used were anti-rat CD3

© 2022 Wiley-VCH GmbH

(G4.18-FITC), CD49a (Ha31/8-BV650), CD49b (Ha1/29-FITC), GATA-3 (L50-823-BV711), T-bet (O4-46-PerCP-Cy5.5, -PE-CF594), and streptavidin-QDot605 from BD Biosciences; Eomes (Dan11mag-PE-Cy7, -Alexa488), RORγt (AFKJS-9-APC), Granzyme A (3G8.5-APC), and streptavidin-QDot585 from ThermoFisher; IFN-γ (DB-1-FITC) from BioLegends; and CD127 (717519-PE) from R&D Systems. Anti-rat mAbs to NKR-P1A (3.2.3-Pacific Blue), CD8α (OX10), CD25 (OX39-biotin), CD93 (LOV3-biotin), CD103 (OX62-biotin), NKG2A/C/E (WEN28-biotin), NKp46 (WEN23-Pacific Blue), Ly49s3 (DAR13-biotin), NKR-P1B (STOK27-biotin, -Alexa700, -PB), CD107a (SIM1-Alexa488), SIRP1α (OX41-Alexa700, -Alexa488), anti-rat kappa chain (OX12-Alexa700, -Alexa488), TCR-αβ (R73-Alexa700) were purified from hybridomas and conjugated in our laboratory. Isotype control antibodies: Rat IgG2a (eBR2A-APC, -PE-Cy7) and mIgG2a (eBB2a-PE) from ThermoFisher; mIgG1 (X40-BV711, -BV650) from BD Biosciences, Franklin Lakes, NJ; and Armenian hamster IgG (HTK888-FITC) from BioLegends.

Intracellular staining for transcription factors was accomplished using BD Biosciences Transcription Factor Buffer Set. Intracellular staining for IFN-γ was performed using the Foxp3 Fixation/Permeabilization kit (eBioscience, San Diego, CA). Cytokines were induced by incubating cells with 1 μg/mL ionomycin and 10 ng/mL PMA (both Sigma-Aldrich) for 4 h, with Golgi Stop (BD Biosciences) added during the last 3 h of incubation. The PrimeFlow RNA Assay kit (ThermoFisher) was used to probe for IL-5 and IL-22 mRNA according to the manufacturer's protocol. In brief, permeabilized cells were hybridized with gene- specific target probes against IL-22 or IL-5 mRNA, followed by preamplifier DNA, amplifier DNA, and finally fluorescent probes to allow single-cell visualization of mRNA by flow cytometry. Cells were analyzed using BDFortessa (BD Biosciences), and data analyzed using FlowJo software.

Degranulation assay

Mononuclear cells from blood, liver, and spleen were incubated with YAC-1 target cells at ratio 1:1 for 4 h at 37°C in cRPMI in the presence of an anti-CD107a antibody. Golgi stop (BD Biosciences) was added after 1 h of incubation. Afterwards, cells were washed and stained with surface markers, and finally transcription factors as described above. Specific degranulation (ΔCD107a) was calculated as the difference in percent CD107a-positive cells against YAC-1 targets versus no targets.

Single-cell RNA sequencing

Mononuclear spleen and liver cells were enriched for innate lymphocytes by depletions using pan-mouse IgG Dynabeads (ThermoFisher) coated with antibodies toward T cells (R73; TCR-αβ), B cells (OX12, Ig-κ), and myeloid cells (ED1; CD68 and OX41; SIRP1-α). Enriched cells were immediately processed for single-cell RNAseq following the Drop-seq protocol by the McCarroll laboratory [49]. In short, the cell suspension was fed through a droplet generator (Dolomite, UK) that encapsulated a single cell and a barcoded bead in a water-in-oil droplet. Following cell lysis inside the droplet, mRNA attached to poly-dT-coated beads were reverse transcribed to make cDNA, amplified, and barcoded fragments generated by Tn5-mediated tagmentation. During the post-tagmentation PCR, unique sample barcodes were introduced in the adaptor primers. The libraries were sequenced at the Norwegian Sequencing Centre (Oslo University Hospital), on the NextSeq500 platform with a 75 bp kit, high output mode, with paired end reads. Twenty base pair was sequenced in Read 1 using a custom sequencing primer (GCCTGTCCGCG-GAAGCAGTGGTATCAACGCAGAGTAC) and 60 bp in Read 2 with the regular Illumina sequencing primer. We used the Drop-seq Core Computational Protocol using STAR alignment to map the raw sequencing data to the most recent version of the rat (BN strain) genome (Rnor_6.0). Reads were then grouped by cell barcode and the unique molecular identifiers for each gene counted. Further analysis was performed in R studio using the Seurat, dplyr, and ggplot2 packages. Initial analysis excluded cells expressing more than 5% mitochondrial genes, or raw counts below 200 or above 2000. A total of 9790 features were present in 689 spleen cells, 7964 features were present in 732 liver cells (replicate 1), and 8770 features in 845 liver cells (replicate 2). The counts were normalized and log-transformed, and principal component analysis based on the feature "FindVariableGenes" with 20 dimensions, followed by clustering and *t*-SNE analysis.

Microbiome analysis

The intestinal microbiome from six 12-week-old male PVG littermates housed in two cages, and three 12-week-old female PVG.7B littermates housed in the same cage were analyzed. All cages were from the same rack. Luminal contents were collected from the jejunum, ileum, cecum, and colon, and frozen at −80°C until analysis. Total DNA was isolated from samples using the QIAamp DNA stool kit (Qiagen) according to the manufacturer's instructions [50], with modifications. Briefly, 100 mg luminal contents were homogenized in 500 μL ASL buffer by bead-beating step using tissue lyzer for 3 min at 30 Hz, followed with 95°C heat-based lysis steps. Then, samples were incubated for 30 min with 200 μL lysis buffer containing 20 mM Tris-HCl, pH 8.0, 2 mM EDTA, 1.2% Triton, and 20 mg/mL lysozyme. A total of 500 μL ASL buffer was added and the manufacturer's protocol continued. Total DNA was eluted in 30 μL RNase-free water and stored at −20°C. The 16S rRNA gene segments spanning the variable V5 and V6 regions were amplified using a multiplex approach with the forward primers containing barcodes (5'-CCAT CTCATCCCTGCGTGTCTCCGACTCAG-BARCODE-ATTAGATACCC YGGTAGTCC-3) in combination with the reverse primer (5'-CCTCT CTATGGGCAGTCGGTGATACGAGCTGACGACARCCATG-3') [50]. The PCR amplified amplicons were purified using Gel Extraction Kit (QIAGEN) as described by the manufacturer's

© 2022 Wiley-VCH GmbH

15214141, 2022, 5, Downloaded from https://onlinelibrary.wiley.com/doi/10.1002/eji.202149639 by Universität Bern, Wiley Online Library on [05/01/2023]. See the Terms and Conditions (https://onlinelibrary.wiley.com/terms-and-conditions) on Wiley Online Library for rules of use; OA articles are governed by the applicable Creative Commons License

15214141, 2022, 5, Downloaded from https://onlinelibrary.wiley.com/doi/10.1002/eji.202149639 by Universität Bern, Wiley Online Library on [05/01/2023]. See the Terms and Conditions (https://onlinelibrary.wiley.com/terms-and-conditions) on Wiley Online Library for rules of use; OA articles are governed by the applicable Creative Commons License

manual and prepared for sequencing on the IonTorrent PGM system (Life Technologies). Data analysis was performed using the QIIME pipeline version 2 [51] with a custom script for IonTorrent data. Amplicon sequencing variants were assigned using Greengenes (13_8) databases using the *feature-classifier classify-sklearn* function with a 97% sequence identity threshold [52]. Calculation of the alpha diversity (Simpson and Shannon index), beta diversity (Bray-Curtis dissimilarities on NMDS plot), and statistical analysis using Adonis test were performed using phyloseq pipeline in R (3.6.3) [51, 53].

Acknowledgments: This study was supported by The Norwegian Research Council (Grant number: 274962, Inngjerdingen).

Conflict of interest: The authors have no conflict of interest.

Ethics approval statement: The use of rats for in vitro research was approved by the local veterinarian at Department of Comparative Medicine, University of Oslo.

Author contributions: AS conceived the study, conducted experiments, analyzed data, and contributed to writing of the manuscript. FMS conducted experiments and analyzed data; BY conducted experiments, analyzed data, and contributed to the manuscript. NCG conducted experiments and analyzed data, AJM analyzed data and contributed to the manuscript, ED analyzed data and contributed to the manuscript. SWX conducted experiments, analyzed data and contributed to the manuscript; MI conceived the study, analyzed data, and wrote the manuscript.

Peer review: The peer review history for this article is available at https://publons.com/publon/10.1002/eji.202149639

Data availability statement: The data that support the findings of this study are openly available in "figshare" at https://doi.org/10.6084/m9.figshare.18913091 (scRNA-Seq) and https://doi.org/10.6084/m9.figshare.17429489 (16S sequencing).

References

1 **Vivier, E., Artis, D., Colonna, M., Diefenbach, A., Di Santo, J. P., Eberl, G., Koyasu, S. et al.**, Innate lymphoid cells: 10 years on. *Cell* 2018. **174**: 1054–1066.

2 **Stehle, C., Hernández, D. C. and Romagnani, C.**, Innate lymphoid cells in lung infection and immunity. *Immunol. Rev.* 2018. **286**: 102–119.

3 **Gasteiger, G., Fan, X., Dikiy, S., Lee, S. Y. and Rudensky, A. Y.**, Tissue residency of innate lymphoid cells in lymphoid and nonlymphoid organs. *Science* 2015. **350**: 981–985.

4 **Di Censo, C., Marotel, M., Mattiola, I., Müller, L., Scarno, G., Pietropaolo, G., Peruzzi, G. et al.**, Granzyme A and CD160 expression delineates ILC1 with graded functions in the mouse liver. *Eur. J. Immunol.* 2021. **51**: 2568–2575.

5 **Friedrich, C., Taggenbrock, R. L., Doucet-Ladevèze, R., Golda, G., Moenius, R., Arampatzi, P., Kragten, N. A. et al.**, Effector differentiation downstream of lineage commitment in ILC1s is driven by Hobit across tissues. *Nat. Immunol.* 2021. **22**: 1256–1267.

6 **Meininger, I., Carrasco, A., Rao, A., Soini, T., Kokkinou, E. and Mjösberg, J.**, Tissue-specific features of innate lymphoid cells. *Trends Immunol.* 2020. **41**: 902–917.

7 **Riggan, L., Freud, A. G. and O'Sullivan, T. E.**, True detective: Unraveling group 1 innate lymphocyte heterogeneity. *Trends Immunol.* 2019. **40**: 909–921.

8 **Bernink, J. H., Mjösberg, J. and Spits, H.**, Human ILC1: to be or not to be. *Immunity* 2017. **46**: 756–757.

9 **Di Vito, C., Mikulak, J. and Mavilio, D.**, On the way to become a natural killer cell. *Front. Immunol.* 2019. **10**: 1812.

10 **Marquardt, N., Kekäläinen, E., Chen, P., Lourda, M., Wilson, J. N., Scharenberg, M., Bergman, P. et al.**, Unique transcriptional and protein-expression signature in human lung tissue-resident NK cells. *Nat. Commun.* 2019. **10**: 1–12.

11 **Allan, D. S., Cerdeira, A. S., Ranjan, A., Kirkham, C. L., Aguilar, O. A., Tanaka, M., Childs, R. W. et al.**, Transcriptome analysis reveals similarities between human blood CD3− CD56 bright cells and mouse CD127+ innate lymphoid cells. *Sci. Rep.* 2017. **7**: 3501.

12 **Mjösberg, J. M., Trifari, S., Crellin, N. K., Peters, C. P., Van Drunen, C. M., Piet, B., Fokkens, W. J. et al.**, Human IL-25-and IL-33-responsive type 2 innate lymphoid cells are defined by expression of CRTH2 and CD161. *Nat. Immunol.* 2011. **12**: 1055.

13 **De Grove, K. C., Provoost, S., Verhamme, F. M., Bracke, K. R., Joos, G. F., Maes, T. and Brusselle, G. G.**, Characterization and quantification of innate lymphoid cell subsets in human lung. *PLoS One* 2016. **11**: e0145961.

14 **Simoni, Y., Fehlings, M., Kløverpris, H. N., McGovern, N., Koo, S. -. L., Loh, C. Y., Lim, S. et al.**, Human innate lymphoid cell subsets possess tissue-type based heterogeneity in phenotype and frequency. *Immunity* 2017. **46**: 148–161.

15 **Satoh-Takayama, N., Vosshenrich, C. A., Lesjean-Pottier, S., Sawa, S., Lochner, M., Rattis, F., Mention, J. -. J. et al.**, Microbial flora drives interleukin 22 production in intestinal NKp46+ cells that provide innate mucosal immune defense. *Immunity* 2008. **29**: 958–970.

16 **Sanos, S. L., Bui, V. L., Mortha, A., Oberle, K., Heners, C., Johner, C. and Diefenbach, A.**, RORγt and commensal microflora are required for the differentiation of mucosal interleukin 22–producing NKp46+ cells. *Nat. Immunol.* 2009. **10**: 83.

17 **Sawa, S., Lochner, M., Satoh-Takayama, N., Dulauroy, S., Bérard, M., Kleinschek, M., Cua, D. et al.**, RORγt+ innate lymphoid cells regulate intestinal homeostasis by integrating negative signals from the symbiotic microbiota. *Nat. Immunol.* 2011. **12**: 320–326.

18 **Sonnenberg, G. F., Monticelli, L. A., Alenghat, T., Fung, T. C., Hutnick, N. A., Kunisawa, J., Shibata, N. et al.**, Innate lymphoid cells promote anatomical containment of lymphoid-resident commensal bacteria. *Science* 2012. **336**: 1321–1325.

19 **Kveberg, L., Bäck, C. J., Dai, K. Z., Inngjerdingen, M., Rolstad, B., Ryan, J. C., Vaage, J. T. et al.**, The novel inhibitory NKR-P1C receptor and Ly49s3 identify two complementary, functionally distinct NK cell subsets in rats. *J. Immunol.* 2006. **176**: 4133–4140.

20 **Kveberg, L., Jimenez-Royo, P., Naper, C., Rolstad, B., Butcher, G. W., Vaage, J. T. and Inngjerdingen, M.**, Two complementary rat NK cell subsets,

© 2022 Wiley-VCH GmbH

Ly49s3+ and NKR-P1B+, differ in phenotypic characteristics and responsiveness to cytokines. *J. Leukoc. Biol.* 2010. **88**: 87–93.

21 **Inngjerdingen, M., Kveberg, L. and Vaage, J. T.**, A novel NKR-P1Bbright NK cell subset expresses an activated CD25+CX3CR1+CD62L-CD11b-CD27- phenotype and is prevalent in blood, liver, and gut-associated lymphoid organs of rats. *J. Immunol.* 2012. **188**: 2499–2508.

22 **Sudworth, A., Vaage, J. T., Inngjerdingen, M. and Kveberg, L.**, Frontline science: a hyporesponsive subset of rat NK cells negative for Ly49s3 and NKR-P1B are precursors to the functionally mature NKR-P1B(+) subset. *J. Leukoc. Biol.* 2017. **102**: 1289–1298.

23 **Westgaard, I. H., Berg, S. F., Vaage, J. T., Wang, L. L., Yokoyama, W. M., Dissen, E. and Fossum, S.**, Rat NKp46 activates natural killer cell cytotoxicity and is associated with FcεRIγ and CD3ζ. *J. Leukoc. Biol.* 2004. **76**: 1200–1206.

24 **Abidi, A., Laurent, T., Bériou, G., Bouchet-Delbos, L., Fourgeux, C., Louvet, C., Triki-Marrakchi, R. et al.**, Characterization of rat ILCs reveals ILC2 as the dominant intestinal subset. *Front. Immunol.* 2020. **11**: 255.

25 **Simoni, Y., Fehlings, M., Kløverpris, H. N., McGovern, N., Koo, S. -. L., Loh, C. Y., Lim, S. et al.**, Human innate lymphoid cell subsets possess tissue-type based heterogeneity in phenotype and frequency. *Immunity* 2017. **46**: 148–161.

26 **Robinette, M. L., Fuchs, A., Cortez, V. S., Lee, J. S., Wang, Y., Durum, S. K., Gilfillan, S. et al.**, Transcriptional programs define molecular characteristics of innate lymphoid cell classes and subsets. *Nat. Immunol.* 2015. **16**: 306.

27 **Daussy, C., Faure, F., Mayol, K., Viel, S., Gasteiger, G., Charrier, E., Bienvenu, J. et al.**, T-bet and Eomes instruct the development of two distinct natural killer cell lineages in the liver and in the bone marrow. *J. Exp. Med.* 2014. **211**: 563–577.

28 **Sojka, D. K., Plougastel-Douglas, B., Yang, L., Pak-Wittel, M. A., Artyomov, M. N., Ivanova, Y., Zhong, C. et al.**, Tissue-resident natural killer (NK) cells are cell lineages distinct from thymic and conventional splenic NK cells. *Elife* 2014. **3**: e01659.

29 **Weizman, O. -. E., Adams, N. M., Schuster, I. S., Krishna, C., Pritykin, Y., Lau, C., Degli-Esposti, M. A. et al.**, ILC1 confer early host protection at initial sites of viral infection. *Cell* 2017. **171**: 795–808.

30 **Klose, C. S., Flach, M., Möhle, L., Rogell, L., Hoyler, T., Ebert, K., Fabiunke, C. et al.**, Differentiation of type 1 ILCs from a common progenitor to all helper-like innate lymphoid cell lineages. *Cell* 2014. **157**: 340–356.

31 **Kveberg, L., Sudworth, A., Todros-Dawda, I., Inngjerdingen, M. and Vaage, J. T.**, Functional characterization of a conserved pair of NKR-P1 receptors expressed by NK cells and T lymphocytes in liver and gut. *Eur. J. Immunol.* 2015. **45**: 501–512.

32 **Abou-Samra, E., Hickey, Z., Aguilar, O. A., Scur, M., Mahmoud, A. B., Pyatibrat, S., Tu, M. M. et al.**, NKR-P1B expression in gut-associated innate lymphoid cells is required for the control of gastrointestinal tract infections. *Cellulr. Mol. Immunol.* 2019. **16**: 868–877.

33 **Bal, S. M., Bernink, J. H., Nagasawa, M., Groot, J., Shikhagaie, M. M., Golebski, K., Van Drunen, C. M. et al.**, IL-1β, IL-4 and IL-12 control the fate of group 2 innate lymphoid cells in human airway inflammation in the lungs. *Nat. Immunol.* 2016. **17**: 636–645.

34 **Monticelli, L. A., Sonnenberg, G. F., Abt, M. C., Alenghat, T., Ziegler, C. G., Doering, T. A., Angelosanto, J. M. et al.**, Innate lymphoid cells promote lung-tissue homeostasis after infection with influenza virus. *Nat. Immunol.* 2011. **12**: 1045–1054.

35 **Bernink, J. H., Krabbendam, L., Germar, K., de Jong, E., Gronke, K., Kofoed-Nielsen, M., Munneke, J. M. et al.**, Interleukin-12 and-23 control plasticity of CD127+ group 1 and group 3 innate lymphoid cells in the intestinal lamina propria. *Immunity* 2015. **43**: 146–160.

36 **Krämer, B., Goeser, F., Lutz, P., Glässner, A., Boesecke, C., Schwarze-Zander, C., Kaczmarek, D. et al.**, Compartment-specific distribution of human intestinal innate lymphoid cells is altered in HIV patients under effective therapy. *PLoS Pathog*. 2017. **13**: e1006373.

37 **Eberl, G., Sawa, S., Lochner, M., Satoh-Takayama, N., Dulauroy, S., Berard, M., Kleinschek, M. et al.**, RORγt+ innate lymphoid cells regulate intestinal homeostasis by integrating negative signals from the symbiotic microbiota. *Nat. Immunol*. 2011. **12**: 320–326.

38 **Atarashi, K., Tanoue, T., Oshima, K., Suda, W., Nagano, Y., Nishikawa, H., Fukuda, S. et al.**, Treg induction by a rationally selected mixture of *Clostridia* strains from the human microbiota. *Nature* 2013. **500**: 232–236.

39 **Ivanov, I. I., Atarashi, K., Manel, N., Brodie, E. L., Shima, T., Karaoz, U., Wei, D. et al.**, Induction of intestinal Th17 cells by segmented filamentous bacteria. *Cell* 2009. **139**: 485–498.

40 **Satoh-Takayama, N., Kato, T., Motomura, Y., Kageyama, T., Taguchi-Atarashi, N., Kinoshita-Daitoku, R., Kuroda, E. et al.**, Bacteria-induced group 2 innate lymphoid cells in the stomach provide immune protection through induction of IgA. *Immunity* 2020. **52**: 635–649.

41 **Kernbauer, E., Ding, Y. and Cadwell, K.**, An enteric virus can replace the beneficial function of commensal bacteria. *Nature* 2014. **516**: 94–98.

42 **Li, S., Bostick, J. W., Ye, J., Qiu, J., Zhang, B., Urban, Jr J. F., Avram, D. and Zhou, L.**, Aryl hydrocarbon receptor signaling cell intrinsically inhibits intestinal group 2 innate lymphoid cell function. *Immunity* 2018. **49**: 915–928.

43 **Dillon, S. M., Castleman, M. J., Frank, D. N., Austin, G. L., Gianella, S., Cogswell, A. C., Landay, A. L. et al.**, Inflammatory colonic innate lymphoid cells are increased during untreated HIV-1 infection and associated with markers of gut dysbiosis and mucosal immune activation. *J. Acquir. Immune Defic. Syndr.* 2017. **76**: 431.

44 **Sim, M. J., Rajagopalan, S., Altmann, D. M., Boyton, R. J., Sun, P. D. and Long, E. O.**, Human NK cell receptor KIR2DS4 detects a conserved bacterial epitope presented by HLA-C. *Proc. Natl. Acad. Sci.* 2019. **116**: 12964–12973.

45 **Helgeland, L., Brandtzaeg, P., Rolstad, B. and Vaage, J. T.**, Sequential development of intraepithelial gamma delta and alpha beta T lymphocytes expressing CD8 alpha beta in neonatal rat intestine: requirement for the thymus. *Immunology* 1997. **92**: 447–456.

46 **Inngjerdingen, M., Kveberg, L. and Vaage, J. T.**, A novel NKR-P1B(bright) NK cell subset expresses an activated CD25(+)CX(3)CR1(+)CD62L(-)CD11b(-)CD27(-) phenotype and is prevalent in blood, liver, and gut-associated lymphoid organs of rats. *J. Immunol.* 2012. **188**: 2499–2508.

47 **Boieri, M., Shah, P., Jalapothu, D., Zaitseva, O., Walter, L., Rolstad, B., Naper, C. et al.**, Rat acute GvHD is Th1 driven and characterized by predominant donor CD4(+) T-cell infiltration of skin and gut. *Exp. Hematol.* 2017. **50**: 33–45.

48 **Cossarizza, A., Chang, H. D., Radbruch, A., Abrignani, S., Addo, R., Akdis, M., Andrä, I. et al.**, Guidelines for the use of flow cytometry and cell sorting in immunological studies. *Eur. J. Immunol.* 2021. **51**: 2708–3145.

49 **Macosko, E. Z., Basu, A., Satija, R., Nemesh, J., Shekhar, K., Goldman, M., Tirosh, I. et al.**, Highly parallel genome-wide expression profiling of individual cells using nanoliter droplets. *Cell* 2015. **161**: 1202–1214.

50 **Yilmaz, B., Juillerat, P., Oyas, O., Ramon, C., Bravo, F. D., Franc, Y., Fournier, N. et al.**, Microbial network disturbances in relapsing refractory Crohn's disease. *Nat. Med.* 2019. **25**: 323–336.

51 **Bolyen, E., Rideout, J. R., Dillon, M. R., Bokulich, N. A., Abnet, C. C., Al-Ghalith, G. A., Alexander, H. et al.**, Reproducible, interactive, scalable and extensible microbiome data science using QIIME 2. *Nat. Biotechnol.* 2019. **37**: 852–857.

© 2022 Wiley-VCH GmbH

15214141, 2022, 5, Downloaded from https://onlinelibrary.wiley.com/doi/10.1002/eji.202149639 by Universität Bern, Wiley Online Library on [05/01/2023]. See the Terms and Conditions (https://onlinelibrary.wiley.com/terms-and-conditions) on Wiley Online Library for rules of use; OA articles are governed by the applicable Creative Commons License

52 **McDonald, D., Price, M. N., Goodrich, J., Nawrocki, E. P., DeSantis, T. Z., Probst, A., Andersen, G. L. et al.**, An improved Greengenes taxonomy with explicit ranks for ecological and evolutionary analyses of bacteria and archaea. *ISME J.* 2012. **6**: 610–618.

53 **McMurdie, P. J. and Holmes, S.**, phyloseq: An R package for reproducible interactive analysis and graphics of microbiome census data. *PLoS One* 2013. **8**: e61217.

Abbreviations: **IEL**: intraepithelial lymphocytes · **ILC**: innate lymphocytes · **Lin**: lineage · **LP**: lamina propria · **NCR**: natural cytotoxicity receptor · **SPD**: Sprague–Dawley · **WKY**: Wistar Kyoto

Full correspondence: Dr. Marit Inngjerdingen, Department of pharmacology, Institute of Clinical Medicine, P.O. Box 1057 Blindern, N-0316 Oslo, Norway.
e-mail: mariti@medisin.uio.no

Received: 16/9/2021
Revised: 3/1/2022
Accepted: 24/1/2022
Accepted article online: 31/1/2022

© 2022 Wiley-VCH GmbH

15214141, 2022, 5, Downloaded from https://onlinelibrary.wiley.com/doi/10.1002/eji.202149639 by Universität Bern, Wiley Online Library on [05/01/2023]. See the Terms and Conditions (https://onlinelibrary.wiley.com/terms-and-conditions) on Wiley Online Library for rules of use; OA articles are governed by the applicable Creative Commons License